Study of higher moments of net-strangeness multiplicity distribution using AMPT model and their expectation for net-kaon using sub-ensemble acceptance method

Submitted for the partial fulfillment of the requirement
for the degree of
Master of Science in Physics

by

Rohit Kumar
(Roll No. V22133)

Supervisor

Dr. Amal Sarkar

School of Physical Sciences
Indian Institute of Technology Mandi
Kamand, Mandi - 175075
Himachal Pradesh, INDIA

DECLARATION

I ensure that the entirety of the research presented in the thesis titled **Study of higher moments of net-strangeness multiplicity distribution using AMPT model and their expectation for net-kaon using sub-ensemble acceptance method** is the result of my investigations conducted at the School of Physical Sciences, Indian Institute of Technology Mandi, India, under the guidance of **Dr. Amal Sarkar**. This work has not been submitted elsewhere for any degree or diploma. Proper acknowledgments have been provided wherever the work is based on the findings of other researchers, as per standard academic practice.

Place: Mandi Signature: 

Date: May 5, 2024 Name: Rohit Kumar

ABSTRACT

Quantum Chromodynamics is an amazing theory that describes a wide range of strong interactions using a good set of basic principles. Phase transitions are fundamental and have a crucial role in understanding the behavior of matter. In this report, we have tried to understand the phase transitions of the matter which interacts via strong interaction i.e. QGP. The phase diagram in QCD is a diagram in the chemical potential μ_B and temperature T plane. In contrast to the water phase diagram for which we have a lot of information, the QCD phase diagram is still discoverable.

Based on understanding so far researchers have found that there exists at least two different phases of QCD matter: a hadronic phase where quarks and gluons are in the constrained state, and a QGP phase in which they are free to move from each other and unconfined. Lattice QCD calculations suggest a crossover region in the QGP-hadronic phase at $\mu_B \approx 0$. However, phase transition of the first order exists at larger μ_B, as suggested by the Hydrodynamics. Models based on Quantum Chromodynamics suggest that the first-order phase transition should end at a critical point. In the vicinity of a critical point long-range correlation and fluctuations diverge.

One of the key signatures of the QCD critical point is the non-monotonic behavior of fluctuations of higher moments of conserved charges such as net-baryon, net-strangeness, and net charge as a function of the center of mass energy.

In this work, the AMPT default version has been used to study net-strangeness moments. For the present work, the energies have been taken 7.7GeV, 19.6GeV, and 27GeV. Due to experimental limitations, we cannot capture all the particles that emerged from heavy ion collisions. Thus we use non-conserved charges as a proxy for conserved charges. We use net-proton, net-kaon, and net-pion as a proxy for net-baryon(ΔB), net-strangeness(ΔS), and net-charge(ΔQ) respectively. So it becomes a compulsion to study the different observables in statistical models. Volume-independent products of higher-order moments are vital observables of critical points. Studies done very recently using the Sub-Ensemble Acceptance method on the HRG model predict a dependence of higher-order moments on experimental acceptance. Here the behaviour of net-strangeness has been analyzed for various volume fractions. We have analyzed cumulants of net-kaon and net-strange multiplicity and their correlation using the Sub-Ensembles Acceptance Method.

Contents

Chapter 1

Introduction

1.1 Phase Transition

Transition from one phase to another is a physical phenomenon in which changes in external conditions cause matter to shift from one physical state to another. The Ehrenfest phase transition suggests that transitions can be broadly divided into three groups [1]: First order, Second order, and Crossover. A discontinuity in the first derivative of free energy concerning a thermodynamic parameter is present in the first-order phase transition(FOPT). These kinds of phase transitions result in the absorption of latent heat. For the second-order phase transition(SOPT), there is a discontinuity in the second-order derivative of free energy. The lower derivative is continuous, though. Crossover is characterized by a smooth transition between phases since there is no discontinuity in the free energy and its derivative. The water phase diagram is a basic illustration of a phase transition. Water phases can change from liquid to gas and from liquid to freeze. Fig. 1.1 displays a basic phase transition diagram.

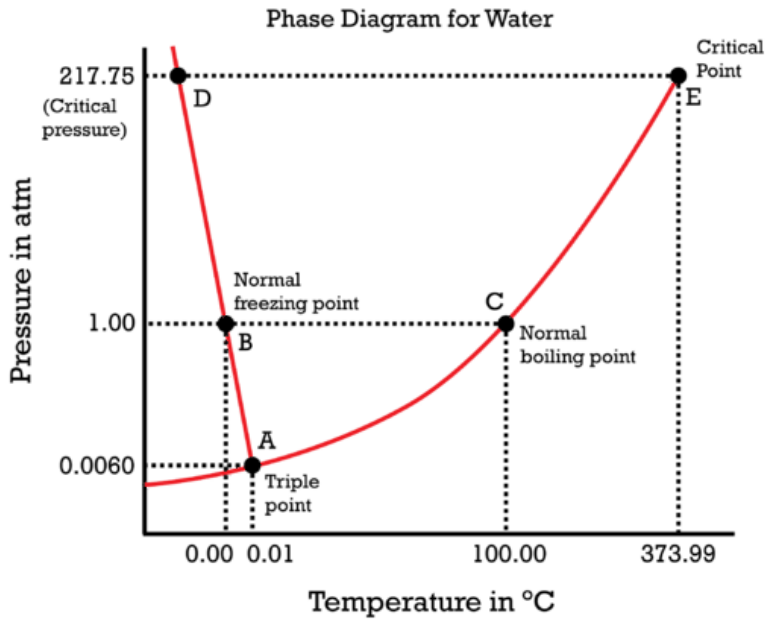

Figure 1.1: Water Phase Diagram

As per Ehrenfest's categorization, the phase transition occurring on the co-existence line is characterized by FOPT. It is explained by the discontinuity in density w.r.t. free energy. Interesting behavior is at the critical point (374° C, 218 atm). It is SOPT. Beyond the critical point, there is a Crossover region and both phases co-exist.

In critical phenomena, the correlation length is a fundamental concept that characterizes the spatial extent of correlations between the microscopic degrees of freedom of a system near its critical

point. As a system approaches its critical point, where a phase transition occurs, fluctuations become increasingly correlated over longer distances. The correlation length represents the typical distance over which these correlations persist.

The critical behavior agrees with the blowing up of the correlation length. Large correlation length develops long-range fluctuations.

1.2 Phase Transition in QCD

Quantum chromodynamics is a reliable theory that explains the strong interaction, one of the four basic interactions in nature. It is a non-Abelian gauge theory that follows **SU(3)** symmetry. As the theory of QED explains the interaction between electric charge(Q), in the same manner, the theory of QCD explains the interaction of color-charges. Like in the QED the photon couples in QED with electric charge with coupling constant $(\alpha = 1/137)$, the gluons couples in QCD with color charge with coupling constant α_s [2]. The running coupling constant is defined as follows:

$$\alpha_s(Q^2) = \frac{12\pi}{(11n_c - 2n_f)ln(|Q^2|/\Lambda^2)} \tag{1.1}$$

where Q^2 is the transfer of momentum, n_c no. of color quarks, n_f no. of quark flavours and Λ is a scaling factor.

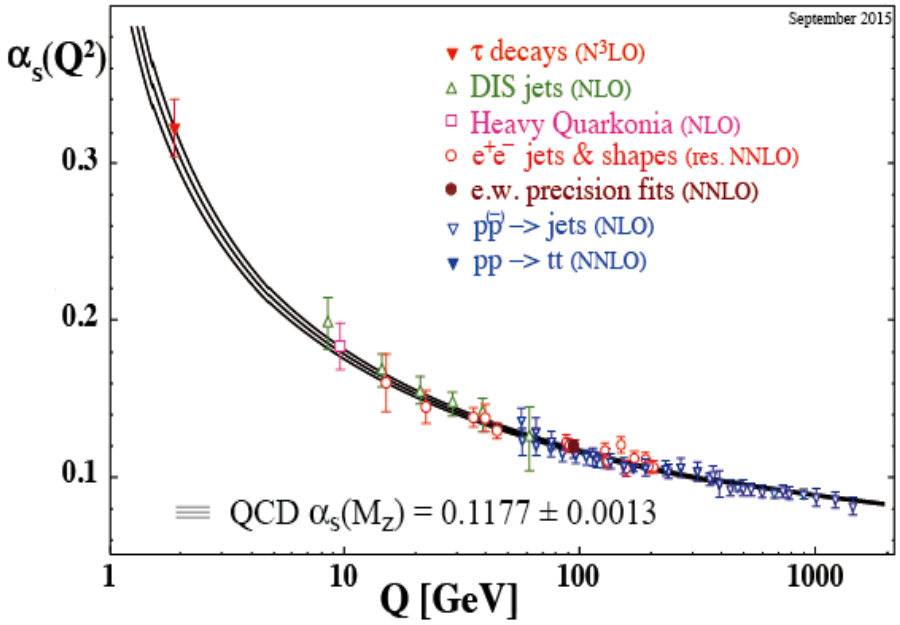

Figure 1.2: Running Coupling constant in QCD [3]

The Q^2 dependence in fig. 1.2 results in two important phases: At larger Q^2 and smaller distances the coupling constant becomes much less which results in the free state of quarks and gluons. This phenomenon is called **asymptotic freedom**. Asymptotic freedom underpins our understanding of the interaction of quarks and gluons in the hadrons and the formation of quark-gluon plasma. At smaller Q^2 the running coupling constant becomes stronger and binds up the quarks and gluons together. This property is called confinement. Hence the fundamental interaction in QCD causes the transition from a constrained state of deconfinement. So if the energy changes then QCD matter switches from one state to another.

1.3 Phase Diagram of QCD

Cabibbo and Parisi proposed the QCD Phase diagram for the first time in their 1975 work [4], which depicted the quarks' transition from a confined to a deconfined state. Even though our understanding of the QCD phase diagram has grown over time, there are still many features that can be found.

The Phase Diagram in QCD is in the plane of temperature T and baryon chemical potential μ_B.

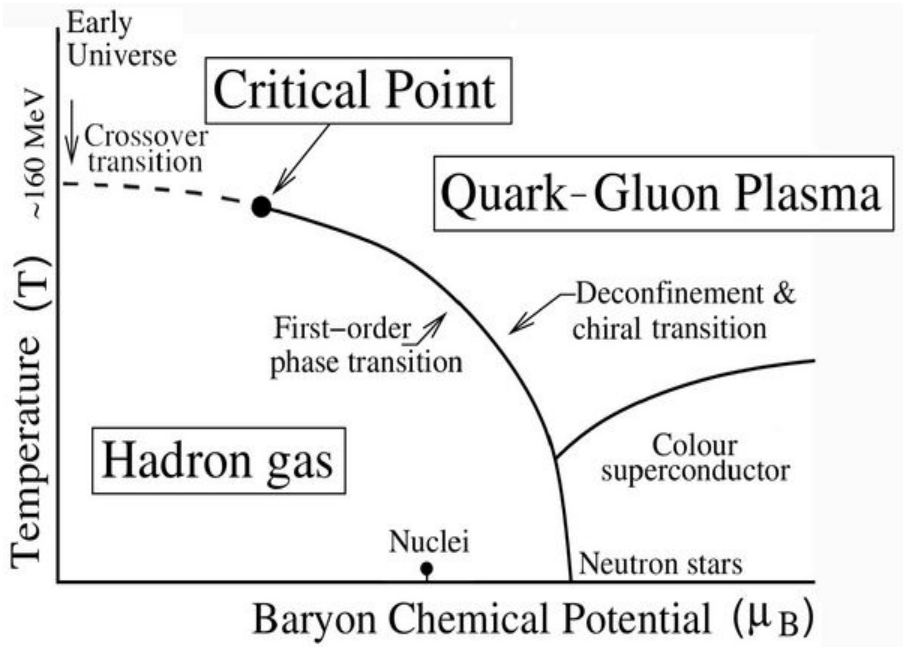

Figure 1.3: Running Coupling constant in QCD

The Phase diagram of strong interaction is shown in the figure 1.3. The solid line shown in the graph is the first-order transition line corresponding to the higher value of μ_B and separating the confined and deconfined phases of QCD matter [5].

At the crucial endpoint, the first-order phase transition line ends and displays a second-order transition. Constrained and deconfined matter coexist in the crossover zone represented by the dotted line at lower μ_B. Neutron stars are extremely dense states of matter that exist at very low temperatures and high baryon density. The following is the relationship of thermal characteristics on the center of mass energy, as determined by statistical model simulations. [6]:

$$\mu_B = \frac{a}{1 + b\sqrt{s_{NN}}} \tag{1.2}$$

where a and b are fitting parameters.

$$T(\mu_B) = n_1 - n_2\mu_B^2 - n_3\mu_B^4 \tag{1.3}$$

here also n_1, n_2 and n_3 are fitting parameters. The above equations clearly show that thermal parameters depend on energy. Changes in energy cause changes in temperature and chemical potential and the phase diagram can be scanned. The observables for CEP are the higher-order moments of the conserved charges multiplicity distribution in QCD. They depend on the correlation length of the system. Near the critical point, fluctuations become correlated for a long range. So Higher order moments show fluctuations near the critical point.

1.4 Higher-Order Moments

In statistics, the moments of a distribution indicate the shape of the distribution. The mean of a distribution determines its peak point. The variance (σ^2), the central moment of the second order, indicates the "spread" of the distribution. Higher-order central moments, skewness (S) and kurtosis (κ), explain the distribution's tail and peak, respectively. A distribution can be defined by its moments, including mean (M), variance (σ^2), skewness (S), and kurtosis (κ). [7].

If f(x) is continuous function of real variable then n^{th} order moment around $\bar{x}$ is defined as:

$$M_n = \int_{-\infty}^{\infty} (x - \bar{x})^n f(x)\, dx \tag{1.4}$$

If one calculated the moments around the mean then they are minimum and called central moments, if μ is the mean then central moments are :

$$M_n = E[(x - \bar{x})^n] = \int_{-\infty}^{\infty} (x - \bar{x})^n f(x)\, dx \tag{1.5}$$

If we divide n^{th} order central moments with n^{th} power of standard deviation (σ^n) these are called normalized moments. Normalized central moments of the third and fourth order are skewness (S) and kurtosis (κ).

Skewness (S): Skewness explains the asymmetry in the distribution. It gives details about the tails of the PDF. it is defined as:

$$S = \frac{E[(x - \bar{x})^3]}{E[(x - \bar{x})^2]^{3/2}} = \frac{M_3}{M_2^{3/2}} \tag{1.6}$$

Fig. 1.4 illustrates that distribution with a higher tail on its left is considered negatively skewed. A distribution with a higher tail on the right is considered positively skewed

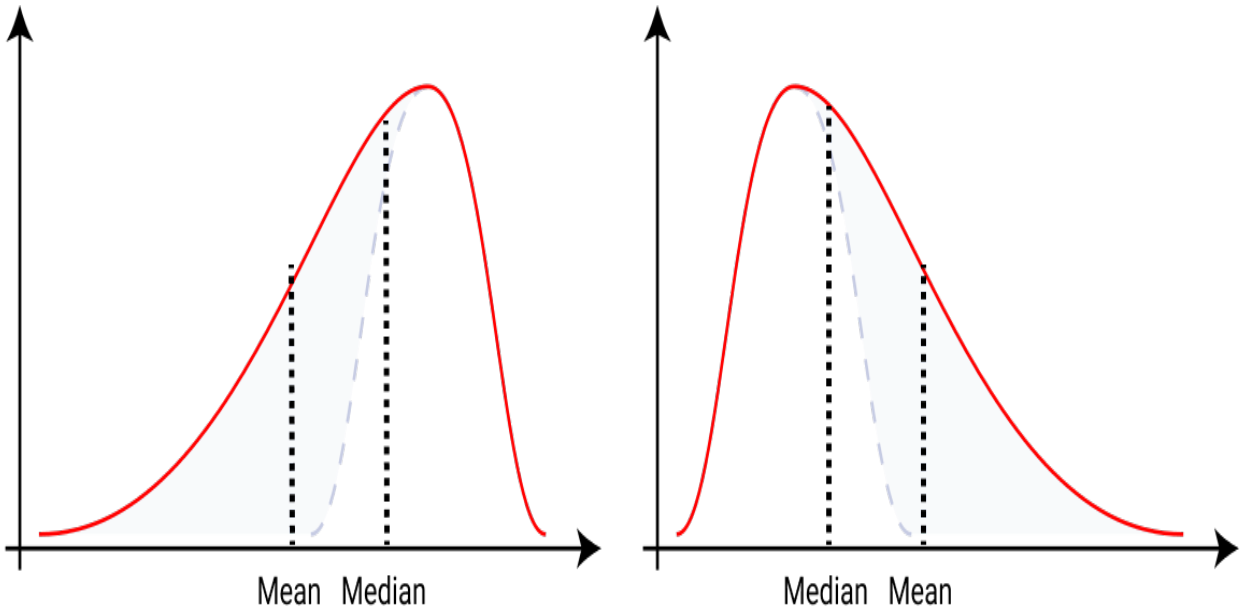

Figure 1.4: measure of skewness: negatively skewed (left panel), positively skewed (right panel)

Kurtosis (κ): The kurtosis of some distribution is interpreted as:

$$\kappa = \frac{E[(x-\bar{x})^4]}{E[(x-\bar{x})^2]^2} - 3 = \frac{M_4}{M_2^2} - 3 \tag{1.7}$$

The kurtosis tells us about the ”peakedness” of the distribution.

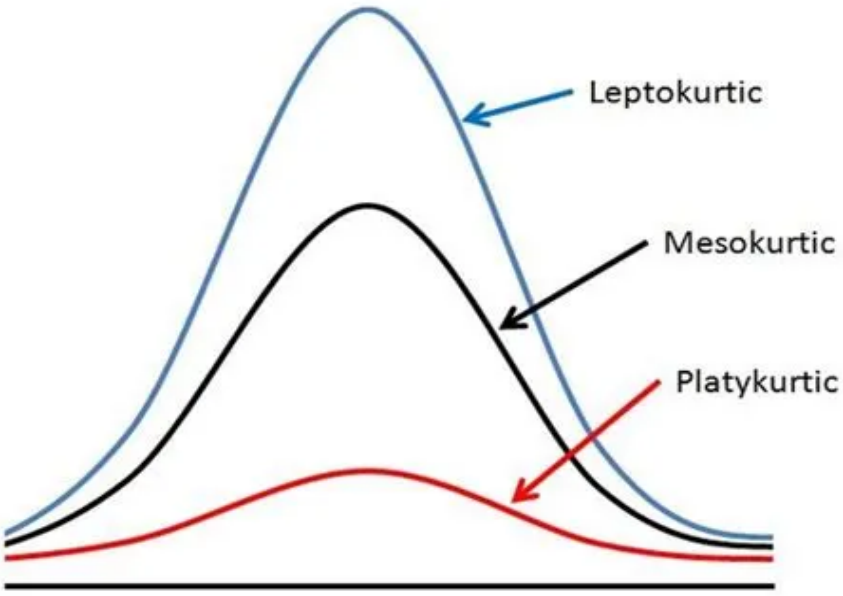

Figure 1.5: Type of distribution for different kurtosis [8]

As shown in Fig. 1.5 if a distribution function has positive kurtosis then it is called ”Leptokutic”. These types of distribution functions have higher peaks than the normal distribution. If the distribution has zero kurtosis then it is called ”Mesokutic”, and the peaks of distribution are the same as Normal distribution. In the case of a distribution function whose kurtosis is negative called ”platykuritc”, and its peaks are flatter than Normal distribution.

1.5 Cumulants

In Probability and Statistics, cumulants are nothing but just an alternative route to moments. If we have two distributions whose moments are the same then their cumulants will also be the same. The cumulants are explained as [9]:

$$b_n = \frac{\partial^n}{\partial t^n} f(t)|_{t=0} \tag{1.8}$$

The expression takes $f(t)$ as the cumulant generating function, with cumulants representing the coefficients of its Taylor series expansion around $t = 0$ [9] :

$$f(t) = tb_1 + \frac{t^2 b_2}{2!} + \frac{t^3 b_3}{3!} + ... + \frac{t^n b_n}{n!} \tag{1.9}$$

Relation between Moments and Cumulants: The Moments and Cumulants are related to each other. Lower-order moments are directly connected to cumulants but 4^{th} and higher-order moments are connected via complex relations. One can relate the cumulants by a recursion formula as follows:

$$b_k = M_k - \sum_{n=1}^{k-1} \binom{k-1}{n-1} b_n M_{k-n} \tag{1.10}$$

where b_k and M_k are n^{th} order cumulants and moments respectively. So now one can write n^{th} order moments for $n \geq 2$ as :

$$\begin{aligned} b_2 &= M_2 \\ b_3 &= M_3 \\ b_4 &= M_4 - 3M_2^2 \\ b_5 &= M_5 - 10M_3M_2 \\ b_6 &= M_6 - 15M_4M_2 - 10M_3^2 + 30M_2^3 \end{aligned} \tag{1.11}$$

1.6 Relation of Higher Moments to Thermodynamic Quantities in Lattice QCD

In thermodynamics, we deal with three types of systems: micro-canonical, canonical, and grand canonical ensemble. In a micro-canonical ensemble, the number of particles and their energy are fixed. A canonical ensemble, also known as a standard ensemble, has a fixed particle number but variable energy. In the case of the grand canonical ensemble, both energy and particle number change.

Let $f_N(V,T)$ be the partition function of CE then the partition function of GCE will be:

$$f(z,V,T) = \sum_{N=0}^{\infty} z^N f_N(V,T) \tag{1.12}$$

where $z = exp(\mu/KT)$ known as fugacity and μ is the chemical potential.

The average particles in the system will be:

$$\begin{aligned} \langle N \rangle =& \frac{\sum z^N f_N}{\sum z^N f_N} \\ &= z\frac{\partial}{\partial z} lnf(z,V,T) = kT\frac{\partial}{\partial \mu} lnf(T,z,V) \end{aligned} \tag{1.13}$$

the mean of the square of the ensemble will be :

$$\langle N^2 \rangle - \langle N \rangle^2 = (kT)^2 \frac{\partial^2}{\partial \mu^2} lnf(T,z,V) \tag{1.14}$$

In QCD, if we take the derivative of dimensionless pressure then we can write susceptibility of conserved charge for n^{th} order as [10] :

$$\chi_q^n = \frac{1}{VT^3} \frac{\partial^n lnf}{\partial(\mu_q/T)^2} \tag{1.15}$$

where $q = (B,Q,S)$

from equations 1.14 and 1.15 and 1.16 one can write :

$$\begin{aligned} \langle N \rangle &= VT^3 \chi_q^{(1)} \\ \langle (\delta N)^2 \rangle &= \langle N^2 \rangle - \langle N \rangle^2 = VT^3 \chi_q^{(2)} \end{aligned} \tag{1.16}$$

similarly, for 3^{rd} and 4^{th} order we can write :

$$\begin{aligned}\langle(\delta N)^3\rangle &= VT^3\chi_q^{(3)} \\ \langle(\delta N)^4\rangle &= VT^3\chi_q^{(4)}\end{aligned} \tag{1.17}$$

It is evident from the aforementioned equations that each of these moments depends on volume. It is challenging to measure the volume in experiments. Therefore, ratio of moments can be taken to exclude the effect of fluctuations caused by volume. Because in ratio volume term is cancels out.

$$\begin{aligned}(S\sigma)_q &= \frac{\chi_q^{(3)}}{\chi_q^{(2)}} \\ (\kappa\sigma^2)_q &= \frac{\chi_q^{(4)}}{\chi_q^{(2)}}\end{aligned} \tag{1.18}$$

1.7 Higher Moments in Heavy-Ion Collisions

In heavy-ion collisions, event-by-event net-kaon numbers have been measured using the AMPT Model.

As shown in Fig. 1.6 the net-kaon multiplicity distribution has been shown for $\sqrt{s_{NN}} = 7.7GeV$ for 70-80% centrality.

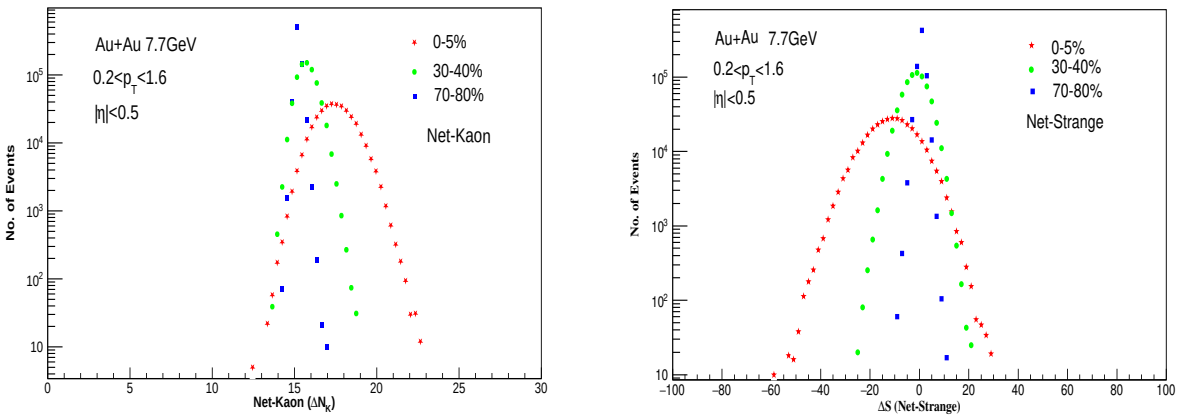

Figure 1.6: Left Panel:net kaon Multiplicity distribution for 7.7GeV, Right Panel: net-Strange multiplicity distribution for different centralities for 7.7GeV

If A represents the number of net-kaon per event then the deviation from the mean is :

$$\Delta A = A - \langle A\rangle \tag{1.19}$$

Here $\langle A\rangle$ is the mean of the particles. Now the cumulants of different order will be :

$$\begin{aligned}C_1 &= \langle A\rangle \\ C_2 &= \langle(\Delta A)^2\rangle \\ C_3 &= \langle(\Delta A)^3\rangle \\ C_4 &= \langle(\Delta A)^4\rangle - \langle(\Delta A)^2\rangle^2\end{aligned} \tag{1.20}$$

Now, the moments as a function for cumulant values are as follows:

$$M = C_1, \sigma^2 = C_2, S = \frac{C_3}{C_2^{3/2}}, \kappa = \frac{C_4}{C_2^2} \tag{1.21}$$

The cumulants are a vital signature for critical endpoint. They depend on the correlation length ρ of the system.They depend as follows $\sigma^2 \propto \rho^2$, $S \propto \rho^{4.5}$ and $\kappa \propto \rho^7$. As we approach the endpoint the correlation length blows up and a fluctuation is observed in volume independent ratio of cumulants.

Chapter 2

A Multi-Phase Transport Model

2.1 Introduction

A multi-phase transport model sometimes referred to as an event generator, is a computational tool in particle physics that is used to mimic particle behavior and interactions in high-energy collisions, like those that take place in particle accelerators like the Large Hadron Collider (LHC). These models are essential for researching the characteristics of matter under severe circumstances, like the heavy-ion collision-produced quark-gluon plasma (QGP). From the starting point of particle generation to the ultimate state, the multi-phase transport model attempts to capture the complete course of a collision event. There are two modes in the model: String Melting Mode (b) and Default Mode (a). The default mode is the one that is being used in this analysis. [11].

It can generate events from 5.5GeV to 5500 GeV for p+A and A+A collisions. The model typically consists of several phases, each representing different stages of the collision process. Here are the key phases commonly incorporated into a multi-phase transport model for default mode:

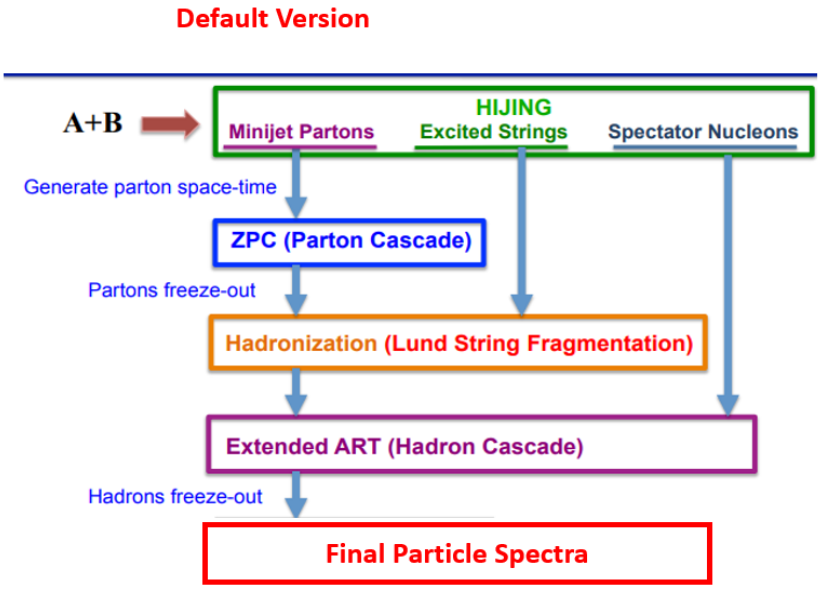

Figure 2.1: Components of Default AMPT Model [12]

2.2 Initial Conditions

Initial conditions in the default AMPT model at RHIC energies are obtained with the help of the HIJING model [13]. The Wood-Saxon density distribution is considered to be the distribution of the radial density profile of two colliding nuclei, and the interaction between nucleons is investigated using eikonal formalism. Treatment will be given to two components: gentle and harsh interactions. Mini jets are manufactured in the hard process under the PYTHIA program's supervision. Excited strings are produced throughout the soft process. The Lund JETSET fragmentation model predicts the independent decay of energized strings. Nuclear Shadowing effects have also been take for the event generation. [14]

2.3 Zhang Parton Cascade (ZPC) Process

The Parton cascade process describes the dynamics and interaction of the partons in the medium produced. In models such as AMPT interaction among partons is taken as their Wigner distribution function which is related to the density distribution of partons. As per ZPC the two partons coming to each other will face a scattering if the distance between them is less than a particular length. In the present scenario, the ZPC includes only two body scatterings in which their cross-sections are calculated using pQCD. [15].

2.4 Hadronisation Process (Lund String Fragmentation)

As mentioned at the start of the chapter there are two modes of the AMPT model: (a) String melting and (b) Default version. The AMPT model uses different schemes for different modes. In the string melting mode quark-coal process is performed for the hadronisation process. But in default mode the process performed for hadronisation is LSD. When the interactions between mini jet partons are seized the formation of strings happens. According to LSD the fragmentation function is in Gaussian form in the transverse momentum. After the formation of hadrons, their positions are calculated using their trajectories[16].

2.5 Hadron cascade (ART Process)

The ART process describes how the medium's interaction between hadrons will evolve. It takes scattering between baryon-baryon, meson-meson, and meson-baryon. The degrees of freedom are taken in terms of isospin for this process. It includes both elastic and inelastic scattering for meson-meson interactions. The starting condition, the contact between the original partons, the interaction between the produced hadrons at the end, and the transition from the partonic to the hadronic phase are known to be significant factors in high energy heavy ion collisions. To the maximum extent feasible, the AMPT model utilizes these procedures. But with so many unknowns, the model is currently more of a simulation tool than a completed code.

2.6 Data Generation

Data generation have been done using default mode of the AMPT model for three different energies 7.7GeV, 19.6GeV and 27GeV. Range of impact parameter have been take from 0-25.60fm. To keep on hadron cascade process NTMAX = 150 have been taken. Value of parameter a and b have been take 0.55 and 0.15 in Lund symmetric splitting function. Popcore mechanism has been kept on for baryon stopping effects. HIJING seed is taken 11 so that every run is different from its previous one.

Chapter 3

Analysis Method

3.1 Centrality Determination

When heavy ions collide near the speed of light at RHIC and LHC a large number of particles are produced. In general, the overlapping between the nuclei engaged in a collision is interpreted as an impact parameter. The impact parameter cannot be measured directly in the experiments. But the more the impact parameter is more particles will produced.

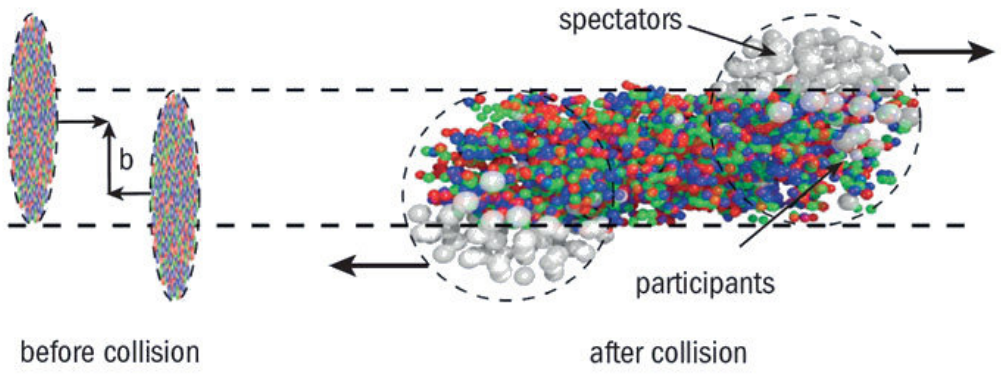

Figure 3.1: An illustrative view of a heavy-ion collision.[20]

N_{part} is the number of nucleons that take part in collisions and N_{coll} is the number of binary collisions.

During the collisions, if the nuclei overlap with each other completely then it is called a head-on collision. It is also termed as 0% centrality. The nucleons which do not take part in collisions are called the spectator nucleons.

Reference multiplicity, meanwhile, is a specific benchmark used within a defined event selection criteria, aiding in the assessment of collision centrality. This centrality measurement provides valuable insights into the extent of overlap between colliding nuclei, crucial for deciphering the physics of the collision.

Figure 3.2 different class of centrality. $0-5\%$ is the top central collisions. And 70-80% are called peripheral collisions.

The primary focus is only on those particles that are the composite particles of strange quarks such as Kaon, lambda zero, omega minus, sigma minus, and sigma plus particles and their antiparticles. There are plots of the number of entries as a function of centrality for each particle at the interval of every 10% centrality.

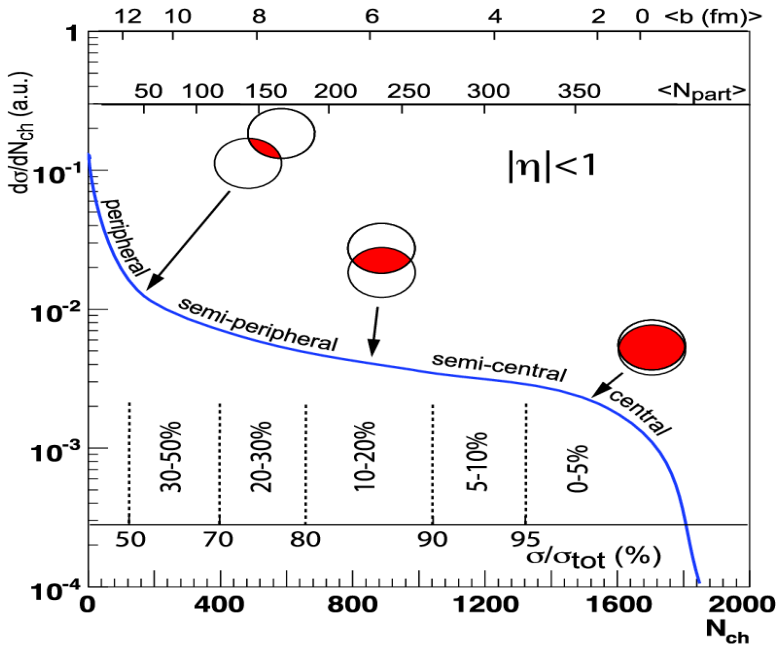

Figure 3.2: Different centrality classes

3.2 Expectation of Net-Strange from Net-Kaon using SAM Model

The subensemble acceptance method is a useful tool for directly comparing theoretical calculations of GCE susceptibilities to higher-order moments of conserved charges measured in central heavy-ion collisions at high energies, where there is a strong position-momentum correlation. It assesses the impact of global conservation regulations. For a tiny acceptance window, dynamical correlations are significantly reduced [17]. As a result, net strangeness are distributed using the Skellam distribution, which is the difference between two independent Poisson distributions. Correlations caused by baryon number conservation, on the other hand, will become relevant as the acceptance to record dynamical fluctuations increases. For a better understanding of large acceptance, the acceptance factor for strange particles is interpreted as the ratio of the average number of captured strange particles $\langle N_S^{acc}\rangle$ to the number of strange particles in full phase space $\langle N_S^{4\pi}\rangle$. Experiments usually analyze on net-kaon higher-order moments which are used as a proxy for the net-strangeness. The acceptance fraction α of the net kaon distribution for strangeness number conservation in a sub-volume can be defined as $\alpha = \langle N_k^{acc}\rangle/\langle N_S^{4\pi}\rangle$, where the mean number of kaon for a particular acceptance is given by $\langle N_k^{acc}\rangle$. The Ratio of 4^{th} order to 2^{nd} order moment $\kappa\sigma^2(\frac{C_4}{C_2})$ for distribution of charge S_1 within the subsystem of the total net Strangeness number, S, is defined by the suggested equation,

$$\frac{C_4[S_1]}{C_2[S_1]} = (1-3\alpha\beta)\frac{\chi_4^S}{\chi_2^S} - 3\alpha\beta(\frac{\chi_3^S}{\chi_2^S})^2 \tag{3.1}$$

where $\beta = 1-\alpha$.

The results after using the SAM extension on the HRG model has been shown in fig. 3.3 It is notable that well-scaled value of second and third-order cumulant is independent of α. As per the prediction of SAM the ratio of any two third order cumulants does not effect by global conservation laws. It is also visible that the denominator for third order cumulant is $(1-2\alpha)$ which diverges for the value of α = 1/2. So there is huge fluctuation for the value of α = 0.5 which is shown if the plot that there is uncertainty for $\alpha = 0.5$. So it is advisable not to do an analysis for the mentioned value of α.

Fig. 3.4 shows the sub-volume acceptance dependence for electric charge (in blue), strangeness number (in red), and baryon number (in black) from MC simulations. The solid line indicates the SAM predictions. It is an interesting observation that fourth-order cumulant value not only depends

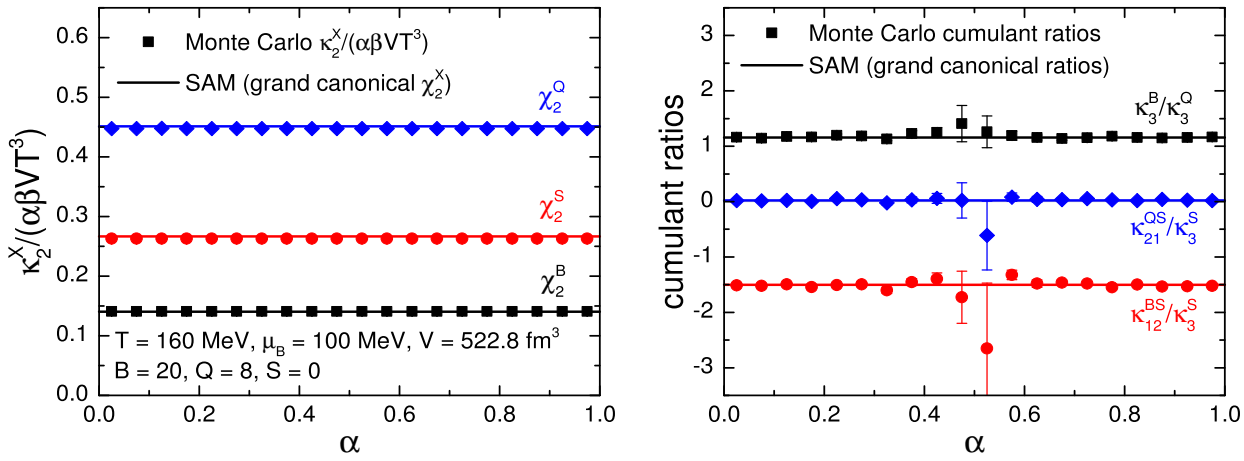

Figure 3.3: Dependence of second order and third order cumulants on α in Monte-Carlo and SAM model is shown in figure Left panel: α dependence of second order cumulant and Right panel α dependence of third-order cumulant [17]

on fourth-order susceptibilities but also depends on the third and second-order susceptibilities. The present behavior should exist at least for $\sqrt{s_{NN}} \geq 39GeV$ because at the higher energies $\mu_B \approx 0$.

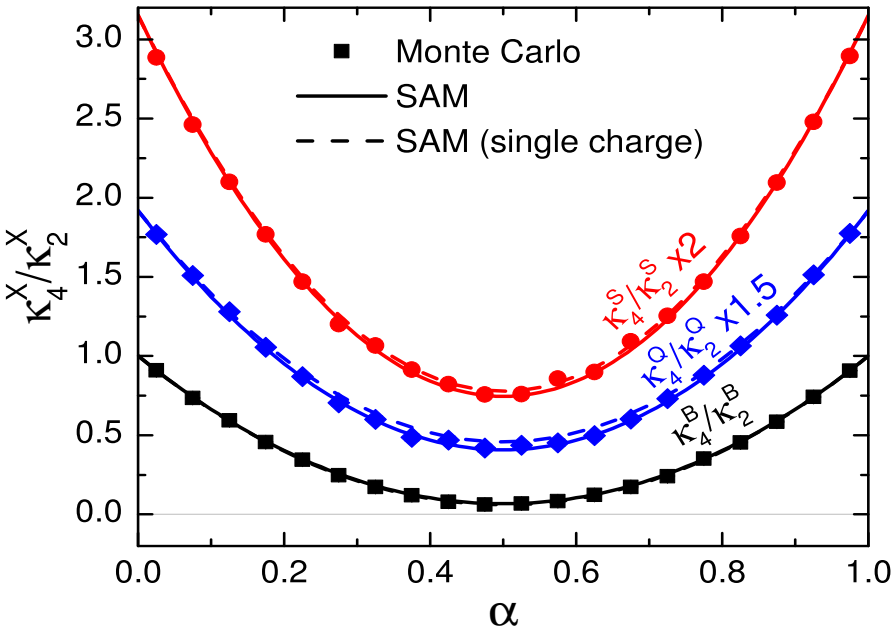

Figure 3.4: Kurtosis cumulant ratio dependence on subvolume fraction α [17]

Chapter 4

Results

4.1 Results and Discussions

Table 4.1: No. of events in different energies

Energy	No. of events (in million)
7.7GeV	7M
19.6GeV	0.9M
27GeV	1M

The number of events generated for different energies has been shown in the tab. 4.1. For particle selection, the cut has been taken as $0.2 < p_T < 1.6$ and $|\eta| < 0.5$. Cumulants up to sixth order and their volume independent ratios($S\sigma, \kappa\sigma^2$ and C_6/C_2) has been calculated. Error estimation has been done using the delta theorem method [18].

In fig. 4.1 the left panel, the graph illustrates C_1 values across various centrality ranges and different energy levels. Notably, in central collisions, the C_1 value appears higher, while it tends to be lower in peripheral collisions. A like trend has been observed in C_2 values.

The plot in the right panel displays C_2 values for nine distinct centrality classes across three different energies in the right panel. However, there are some fluctuations which are statistical fluctuations.

Fig. 4.2 displays the value of third-order and fourth-order moments for different centralities. It is observable that the trend is much like similar in all three energies but some fluctuations are solely due to statistical fluctuations.

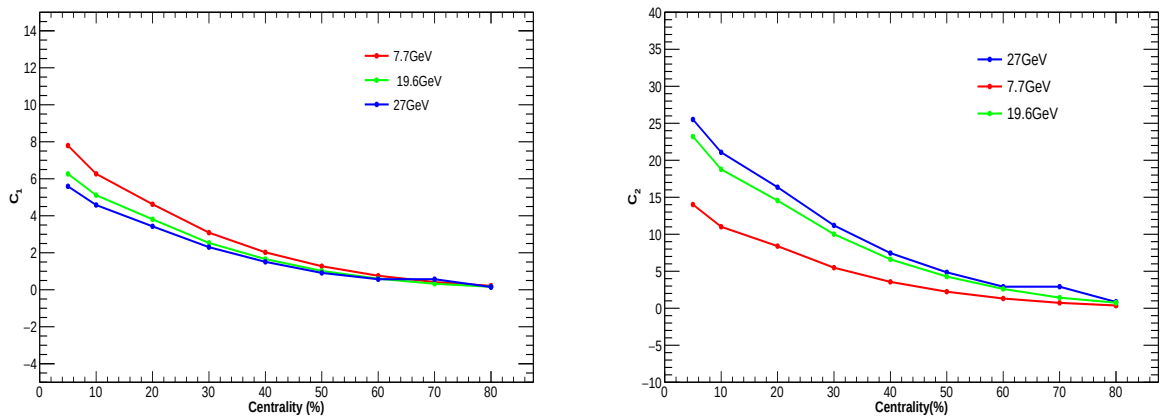

Figure 4.1: Left Panel: C_1 with centrality, Right Panel: C_2 with centrality

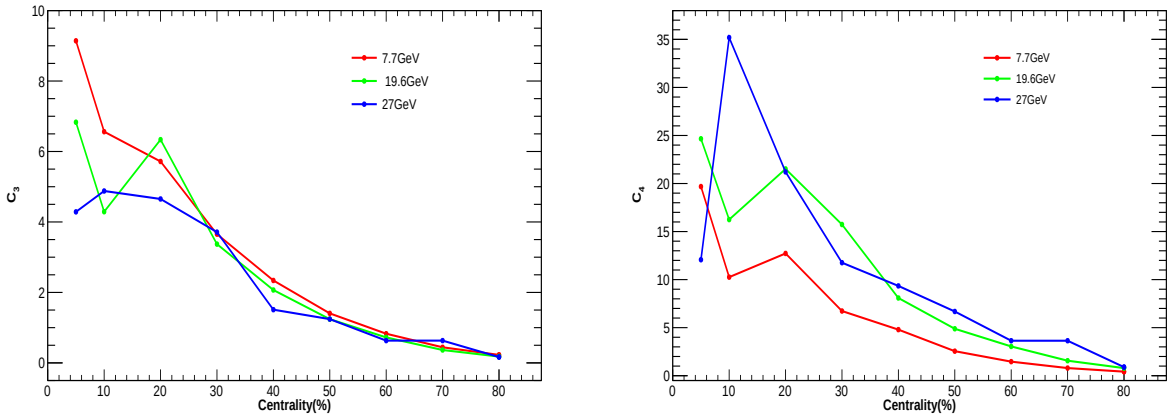

Figure 4.2: Left Panel: C_3 for different centralities, Right panel: C_4 for different centralities

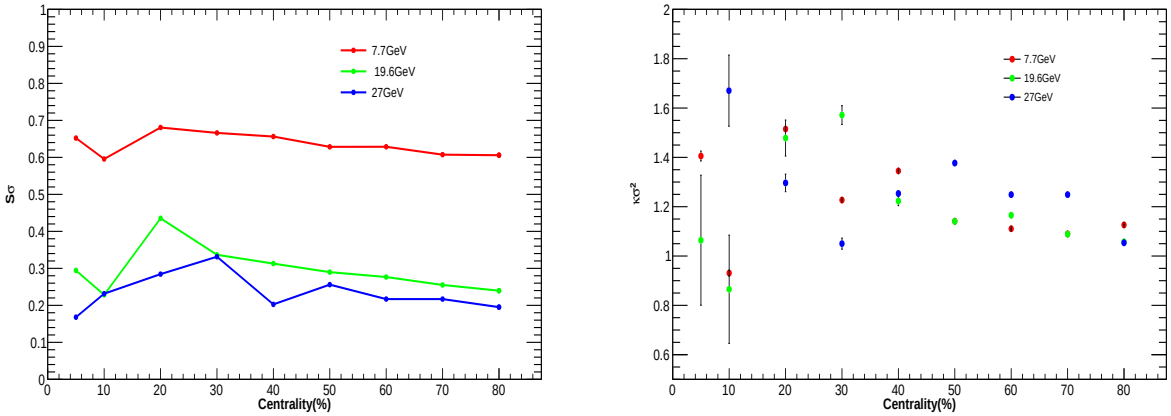

Figure 4.3: Volume independent ratio of cumulants Left Panel: show the C_3/C_2 ratio plots and Right Panel: show the C_4/C_2 ratio plots with errors

In Figure 4.3 the plots represent the volume-independent ratio of cumulants. The distribution of net-kaon multiplicity follows the Skellam distribution, which arises from the difference between two Poisson distributions. The Poisson distribution indeed possesses a unique property wherein the cumulants of order two and higher share identical values, and these cumulants exhibit an additive nature. As a consequence, the ratio of two even cumulants is expected to be unity.

However, recent research has unveiled that fluctuations in the ratio of cumulants can also be attributed to statistical effects. These findings suggest that despite the theoretical expectation of unity for the ratio of even cumulants, observed fluctuations may deviate from this ideal due to statistical variations.

For instance, $\kappa\sigma^2$, which characterizes the variance of particle multiplicity fluctuations, typically requires at least 10 million events to yield statistically reliable results. Similarly, to accurately determine the ratio C_6/C_2, which provides insights into higher-order cumulant fluctuations, an even larger dataset of around 100 million events is often necessary.

In the right panel, the C_4/C_2 plot indicates there are higher fluctuations in central collisions. The reason behind these higher fluctuations is that QGP formed in central collisions is a highly dynamic and evolving system with complex interactions among its constituents. Thermal fluctuations within this system can lead to variations in particle production, momentum distributions, and other observables measured in experiments.

Since AMPT does not contain any information about the critical behavior of strong interaction the

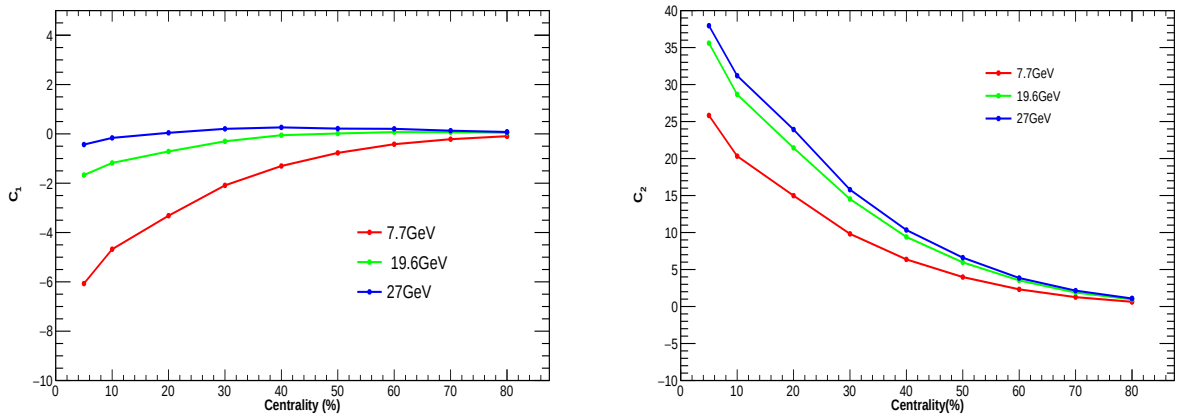

Figure 4.4: C_1 and C_2 distribution of net-strange for nine different centralities, Left panel: describes C_1 behaviour of different centralities and Right Panel: describes C_2 behaviour for different centralities

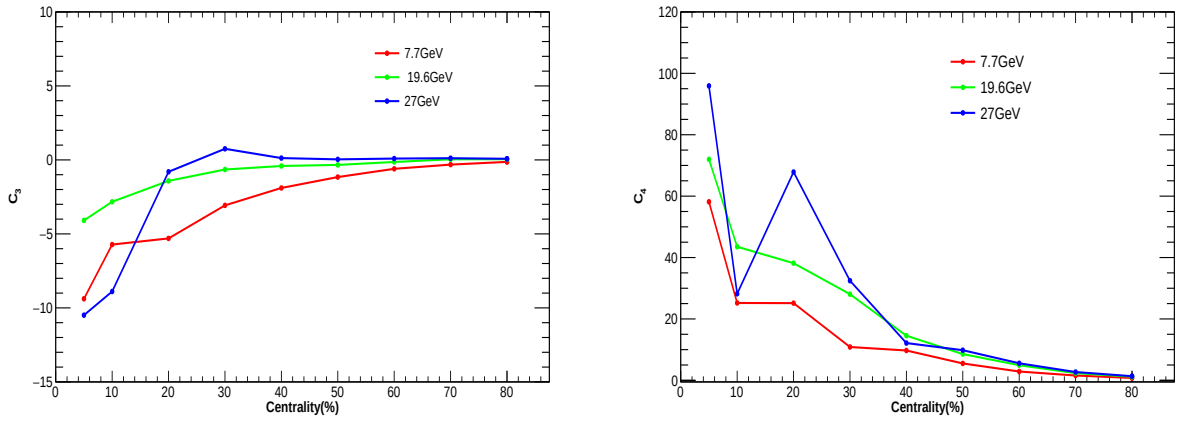

Figure 4.5: C_3 and C_4 distribution of net-strange for nine different centralities, Left panel: describes C_3 behaviour of different centralities and Right Panel: describes C_4 behaviour for different centralities

fluctuations in the cumulants and their volume-independent ratio is due to solely statistical. Indeed, it's worth noting that the fluctuations observed for the energy of 7.7 GeV are comparatively lower than those for the other energies. This discrepancy can be attributed to the higher statistics available for the 7.7 GeV energy level in comparison to the other two energies.

Higher statistics provide a more robust dataset, resulting in reduced statistical uncertainties and fluctuations in the measured quantities. Therefore, the more abundant data available for the 7.7GeV energy level leads to more stable and less fluctuating results in the observed cumulant ratios.

A similar study has also been shown for net-strangeness results. The results have been shown in fig. 4.4 to fig. 4.6 below. It is notable that the trend for net-strange cumulants in different centralities bins is pretty much similar to net-kaon cumulant as explained below. But the value of cumulants is different from the net-kaon cumulants. The reason behind is this that while calculating net-strange cumulants we consider all strange particles which changes the distribution and the values are different. As seen before the behaviour of C_4/C_2 is same is as seen in net-kaon distributions and there is also high fluctuations in central collisions as compared to peripheral collision which is due to system behaviour in the central collisions.

Fig. 4.7 shows the C_6/C_2 variation for net-kaon and net-strange in different centrality bins for different energies. From the figure it is observable that the variation for 7.7GeV in net-kaon and net-strange ratio is similar but for other two energy it is not matching. The reason is that there is higher

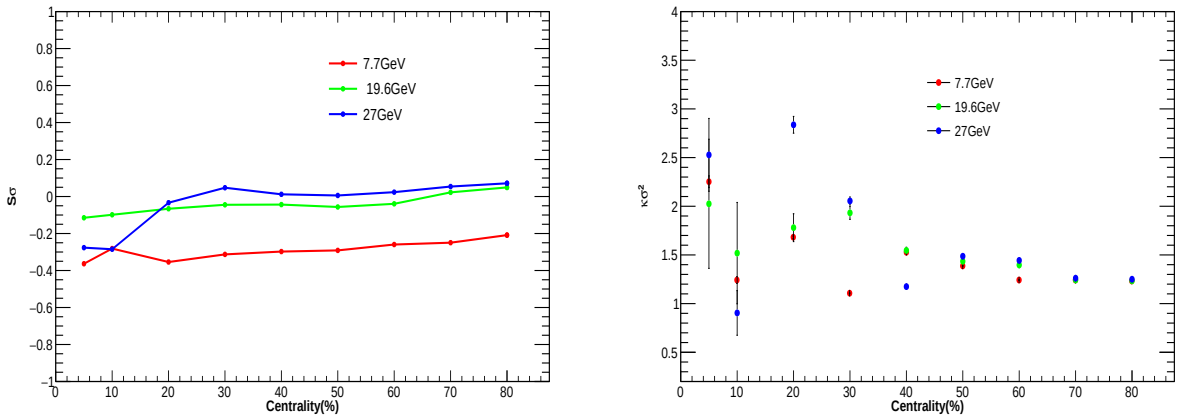

Figure 4.6: Volume independent ratio for different centralities for net-strange Left Panel: C_3/C_2 ratio for different centralities and Right Panel: C_4/C_2 ratio for different centralities

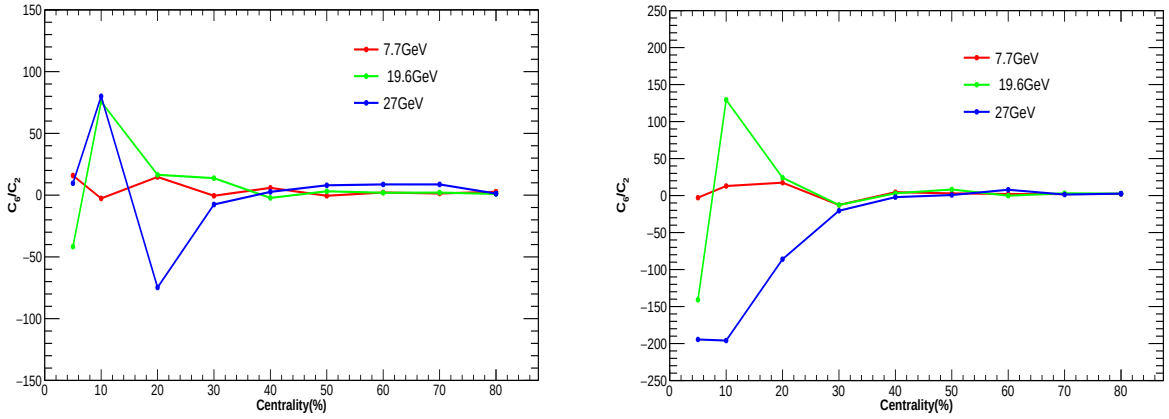

Figure 4.7: C_6/C_2 ratio for different centralities, Left Panel: for net-kaon distribution and Right Panel: for net-Strange distribution

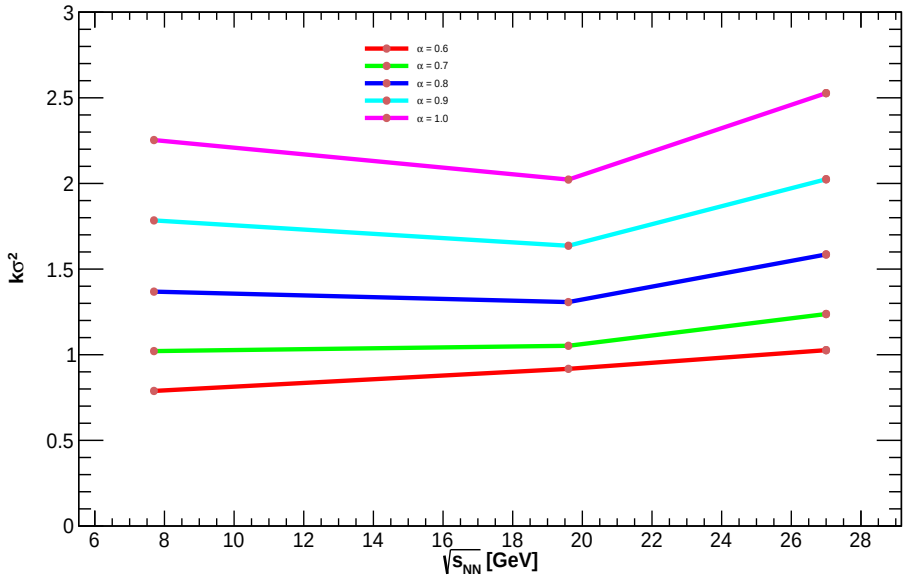

Figure 4.8: α dependence of $\kappa\sigma^2$ for different energies

statistics available in 7.7GeV in comparison for other two energies.

Fig. 4.8 shows the subvolume fraction dependence of $\kappa\sigma^2$ for different enrgies. It is seen that the value of $\kappa\sigma^2$ decrease with decrease in α. The motivation of study is at what fraction results for net-kaon and net-strange should match. Because of the limited statistics currently available, there are large fluctuations, making it challenging to make accurate predictions. A significantly larger amount of data is necessary to improve our understanding of this matching.

4.2 Summary and Outlook

In this report higher order moments net-kaon and net-strangeness for three different energies in different centrality bins using the AMPT model. The study reflects that the fluctuations in higher order moments strongly depends on the statistics. Results for $\sqrt{s_{NN}} = 7.7GeV$ are showing less fluctuation other than 19.6GeV and 27GeV. Because it has much higher statistics available.

Similiarly, the subvolume fraction dependence of $\kappa\sigma^2$ is decreasing with decrease in subvolume fraction. But again due to limited statistics any strong prediction cannot be made for relation between net-kaon and net-strange results.

In the future, more statistics will be generated for all the energies available at RHIC Beam Energy Scan Program and we will compare the theoretical and experimental expectation of net-kaon multiplicity distribution.

ACKNOWLEDGEMENT

I extend my heartfelt appreciation to my guide, **Dr. Amal Sarkar**, for his invaluable guidance and support throughout the project. The learning experience under his guidance has been truly remarkable. I am also grateful to all my lab mates and my senior, Trishu Verma, for their insightful discussions.

Special thanks go to **Dr. Zi-Wei Lin** for his generous assistance in comprehending the AMPT model.

Bibliography

[1] Gregg Jaeger. The ehrenfest classification of phase transitions: introduction and evolution. *Archive for history of exact sciences*, 53:51–81, 1998.

[2] Carlos García Canal. Hera has been closed, lhc is being opened: Near past and near future of particle physics. *Brazilian Journal of Physics - BRAZ J PHYS*, 38, 09 2008.

[3] https://physics.stackexchange.com/questions/311843/physical-observability-of-running-couplings.

[4] Nicola Cabibbo and Giorgio Parisi. Exponential hadronic spectrum and quark liberation. *Physics Letters B*, 59(1):67–69, 1975.

[5] MA Halasz, AD Jackson, RE Shrock, Misha A Stephanov, and JJM Verbaarschot. Phase diagram of qcd. *Physical Review D*, 58(9):096007, 1998.

[6] A Andronic, P Braun-Munzinger, and J Stachel. Hadron production in central nucleus-nucleus collisions at chemical freeze-out. *Nuclear Physics A*, 772(3-4):167–199, 2006.

[7] Wikipedia. Higher Order Moments. https://en.wikipedia.org/wiki/Moment_(mathematics)#:~:text=the%20required%20relationship.-,Higher%20moments,estimation%20of%20further%20shape%20parameters.

[8] medium. "understanding kurtosis and how to determine if your data has a normal distribution". https://medium.com/@dancerworld60/kurtosis-and-how-to-find-given-distribution-is-normal-or-not-50ed3b05bf3b.

[9] Wikipedia. "cumulants". https://en.wikipedia.org/wiki/Cumulant.

[10] Peter Braun-Munzinger, Krzysztof Redlich, and Johanna Stachel. Particle production in heavy ion collisions. In *Quark–Gluon Plasma 3*, pages 491–599. World Scientific, 2004.

[11] Zi-Wei Lin, Che Ming Ko, Bao-An Li, Bin Zhang, and Subrata Pal. Multiphase transport model for relativistic heavy ion collisions. *Physical Review C*, 72(6):064901, 2005.

[12] https://indico.bnl.gov/event/4773/contributions/26332/attachments/21597/29571/AMPT_final.pdf.

[13] Miklos Gyulassy and Xin-Nian Wang. Hijing 1.0: a monte carlo program for parton and particle production in high energy hadronic and nuclear collisions. *Computer Physics Communications*, 83(2-3):307–331, 1994.

[14] Xin-Nian Wang and Miklos Gyulassy. Hijing: A monte carlo model for multiple jet production in pp, pa, and aa collisions. *Physical Review D*, 44(11):3501, 1991.

[15] Bin Zhang. Zpc 1.0. 1: a parton cascade for ultrarelativistic heavy ion collisions. *Computer Physics Communications*, 109(2-3):193–206, 1998.

[16] Bo Andersson, Sandipan Mohanty, and Frederik Söderberg. The lund fragmentation process for a multi-gluon string according to the area law. *The European Physical Journal C-Particles and Fields*, 21(4):631–647, 2001.

[17] Volodymyr Vovchenko, Roman V Poberezhnyuk, and Volker Koch. Cumulants of multiple conserved charges and global conservation laws. *Journal of high energy physics*, 2020(10):1–39, 2020.

[18] Xiaofeng Luo. Error estimation for moment analysis in heavy-ion collision experiment. *Journal of Physics G: Nuclear and Particle Physics*, 39(2):025008, 2012.